A lightweight beak-like sensing system for grasping tasks of flapping aerial robots

Daniel Feliu-Talegón, José Ángel Acosta, Vicente Feliu-Batlle, and Anibal Ollero,

***Abstract*—Many sensor systems in robotics are bio-inspired by similar mechanisms in living creatures. Birds frequently use their beaks to grasp and manipulate objects. This work proposes a very lightweight sensor system that emulates a bird's beak, thus allowing flapping aerial robots to interact with the environment, as e.g. to perform grasping or manipulation tasks. The sensor system is composed of a flexible link (beam) actuated by a micro servomotor, two strain gauges placed on different points and a rigid link opposed. Additionally, a new algorithm is also developed that estimates the instant at which the beak impacts with an object, the contact position and the exerted force. Our sensor system outperforms the existing designs in robotics applications, because it is lightweight, small, cheap, with very low computational load and without any complementary perception. It is demonstrated that the adequate placement of two strain gauges allow the estimation of the contact point and the force exerted between the beam and an object, and the accuracy achieved is enough to reckon properties of the object and develop force control systems. The validation has been made and reported through finite-element simulations and experiments, and the results illustrate the efficiency of the prototype and the proposed algorithm.**

I. Introduction

In the framework of the European project GRIFFIN ERC Advanced Grant [1], this work continues the research and development of limbs and sensing subsystems for flapping-wing robots and, in particular, for the current aerial platform called E-FLAP [2]. As it was thoroughly explained in [2], and unlike all the existing flapping-wing robots, the backbone of this project is to develop a platform with the ability of physical interaction with the environment, to explore the possibility of perching and performing some manipulation tasks once the system is perched. However, the hard challenge of adding E-FLAP functional limb and sensing subsystems has not been resolved yet. Reliable solutions for the robot skeleton with a claw and the non-trivial control problem of manipulating while the system is perched maintaining the equilibrium are provided in [3] and [4], respectively. It is worth mentioning that taking into account the inherent limitations of the system, the control solution provided in [4] has been addressed for the first time.

Flapping-wing robots are a very promising technology that deserves to be deeply explored. These robots outperform other aerial platforms in many aspects. For example, the ability to fly in different modes (flapping, gliding and soaring) can increase flight efficiency by saving energy, and the absence of propellers makes them quieter and safer, allowing operation in close proximity to humans. However, this technology is not mature yet, since it suffers from a hard limitation in size and weight, mainly due to the lack of ultralight structures and its dependence on batteries. This fact impulses the development of lightweight sensor subsystems, i.e. composed of lightweight sensors and actuators. Finally, it is crucial to develop algorithms with low computational load that run on ultralight electronics.

Taking into account those requirements, this work focuses on the development of a sensor subsystem imitating the beak of birds. In Nature, birds use their beaks as an external anatomical structure for killing preys, eating or manipulating objects. The beaks are composed of two jaws, known as the upper and lower mandibles. The proposed sensor subsystem emulates the upper part of the beak with a flexible link with actuation, and the lower part with a rigid link. This is the configuration that uses the minimum number of parts to carry out grasping and manipulation tasks. In particular, the upper part contains a lightweight flexible beam, a micro motor and a pair of strain gauges placed on two different points of the flexible link. Strain gauges are ultralight sensors that, being adequately placed, are very reliable and effective sensors to measure strains, and thus they can be used to estimate force/torques. In fact, flexible links have been recently used in many promising applications as: object identification and spatial localization [5]; texture discrimination in mobile robots [6]; simultaneous localization and mapping techniques for robot navigation [7]; classification of objects based on their material properties [8]; underwater sensing whiskers to measure water flow velocity [9], and as two-flexible-fingers gripper for grasping tasks [10].

The success of grasping with this configuration relies on a good estimate of the contact point of the object with the beak, which can occur anywhere on the mandible. Then it is crucial to know its exact location in order to exert a prescribed force. In most of the force control applications, this location is known or it is assumed that the contact is produced at the tip of the robot (e.g [11] and [10]). This limits the range of operation in the manipulation and reduces its accuracy. Another way to identify the contact location and the contact force is adding a complementary system like computer vision [12]. This increases the weight and complexity of the sensing subsystem and, for this reason, is discarded here.

The main contribution of this work—keeping in mind the requirements described above for flapping aerial robot applications–can be summarized as follows: 1) design and

Manuscript received September, 15, 2021; revised November, 25, 2021.

This work was supported by the European Project GRIFFIN ERC Advanced Grant 2017, Action 788247 and in part by the Grant PID2019-111278RB-C21 funded by MCIN/AEI/ 10.13039/501100011033 and ERDF A way of making Europe and partly by the European Social Fund (FEDER, EU). D. Feliu Talegón, J.Á Acosta and A. Ollero are with the Robotics, Vision and Control Group at the University of Seville (Spain). (e-mail: danielfeliu@us.es; jaar@us.es; aollero@us.es). Vicente Feliu-Batlle is with the Escuela Técnica Superior de Ingenieros Industriales, University of Castilla-La Mancha (UCLM), Ciudad Real (Spain) (e-mail: vicente.feliu@uclm.es)

construction of a lightweight sensor prototype that allows interaction with the environment, based on flexible materials and inspired by the birds beak, and 2) a method to estimate the impact instant, the contact point and the exerted force at the contact point, relying only on the measure from two ultra-lightweight strain gauges. To the best of the authors' knowledge this is the first sensor of this kind. This sensor subsystem outperforms previous works in the following:

1) **Reduced size and weight mechatronics.** The lightweight prototype is the combination of: a flexible link, for a soft interaction with the environment [10]; two ultra-lightweight strain gauges; actuation with high-reduction micro-motor with encoder, in fact, the smallest commercial one available; and a compact electronics. This sensing system constitutes then a feasible solution for force control in aerial robotics, unlike conventional heavy force-torque sensor combinations (see e.g. [13] and [14]). More importantly, no complementary perception system is needed.
2) **New force estimation method including gravity.** The method estimates the position of the contact point and the force exerted there, based on the steady-state deflection measurements of the flexible link. This makes the estimation very simple and with a very low computational demand. Unlike other methods, real time estimation of the natural frequencies of the beam is not needed, which can be very tedious. Moreover, our method considers the gravity effect showing its importance in our application what distinguish us from other former methods (e.g. [15]).

The paper is organized as follows. Section II is devoted to the related works. Section III presents the dynamic model of the system. Section IV explains the developed methods. Section V shows the experimental prototype, some simulations obtained with a finite element software and the experimental results. Finally, some conclusions are given in Section VI.

II. Related works

This section describes some already existing sensing systems and the methods that they use to estimate the impact instant and the contact point distance. The technology to estimate the location of an impact/contact point in real time in a slender flexible link has been mainly developed in the context of the research on robotic sensing antennae.

One of the first results in this subject was proposed in [16]. The proposed sensing system was composed of a flexible link that moved in a horizontal plane, a torque sensor, a joint position sensor, a rotational actuator, and a payload at the tip end of the link. The contact point of the antenna with the environment was determined by measuring the natural frequencies of the links oscillations during the contact mode. It was proved that only using the fundamental and the second natural frequencies is sufficient to uniquely determine the contact point of the antenna with the environment provided that: the link has uniform mass and stiffness distributions; and a light payload is added at the endpoint of the antenna in order to avoid the indeterminacy. Experiments demonstrated that it is a very useful sensing strategy, and reported estimations of the contact point of the link with relative errors about 3% of its length.

Another former approach was given in [13], where a sensing antenna composed of a flexible link, two rotational motors for 3D movements, joint position sensors installed in the motors, and a six-axis force/moment sensor placed at the base of the link was developed. This sensing system finds the contact location as the quotient between the measured moment and force. This paper considers gravity and lateral slip in the estimation. Results show contact point estimations with relative errors about 1-5% of the length of the antenna.

A sensing whisker was built by [17]. The setup was similar to the one of [13], but with a link much more flexible. The link sweeps around the unknown object determining the three-dimensional location of contact points. Experiments reported relative errors about the 3% of the length of the link.

Another antenna prototype similar to [13] was developed in [14]. The only difference was that a payload was added at its tip. It combined an estimator of the impact instant with an estimator of the contact point based on the static information provided by the forces and torques measured by the six-axis force/moment sensor placed at the base of the link [18]. The results reported relative errors of 3% of the length of the antenna. Subsequently, the tip payload was removed and its link was replaced by a nearly twice longer link in [19]. The results reported similar relative errors (3% of the length of the antenna) but without the need of adding a mass at the tip and increasing the workspace of the system.

Finally, in [20], a contact point estimator that combines static and dynamic information of the six-axis force/moment sensor placed at the base of the link was proposed. The method proposes a fusion of the information provided by two of the previous strategies: the one that uses the natural frequencies of vibration of the antenna [16] and the one that uses the static information provided by the forces and torques measured at the base of the antenna. This method improves the accuracy in the estimation up to 2% of the length of the antenna and is valid for horizontal and vertical movements.

Recently, another approach was proposed to estimate the contact point in an artificial tapered whisker sensor by inspecting the strain according to a specific angular displacement [15]. They demonstrate the unique correlations among strain, contact distance and angular displacement. However, this method does not consider the effect of gravity and, thus, it is discarded for our application. It is important to highlight that none of the aforementioned works estimate the exerted force between the flexible link and the environment. They only focus their attention in the estimation of the contact distance.

Aforementioned systems need to detect efficiently the collision of the robot with an object. This detection has to be accurate in order to stop immediately the robot reducing the damage of the impact or, in applications where the robot has to interact with the environment, to switch from position to force control. Several algorithms are already available in the literature. They are based on detecting when either a measured torque or its residue, i.e, the difference between the measured torque and its value predicted by a model, exceed a threshold: [21] and [22] for rigid and [11] and [23] for flexible link

robots. Based on the same principle, efficient algorithms have recently been developed that detect the impact instant of a sensing antenna with an object [19] and [24]. These algorithms are needed to control robots that interact with the environment. For example, in [25] one of the algorithms was used to achieve force control with robustness to uncertainties in the environment.

All the methods described above fail to meet the requirements of our application, mainly because of the their size, their weight (they use heavy force-torque sensors or require a small payload at the tip), not considering the gravity or, more importantly, they are antennas/whiskers and hence not able to grab objects with the necessary size. Therefore, these are the *raison d'être* of the present work.

III. Dynamic model of the bird's beak

The upper mandible of the beak is made of an elastic material and can be modelled as a flexible link that deflects as a function of the contact point of the mandible with the grasped object and the force exerted on it. The lower mandible is a rigid link. Fig. 1 shows a simplified scheme of our robotic beak. Our sensing system measures the deflection at two points of the upper mandible using strain gauges, as depicted and colored in Fig. 1. In this way, we aim at estimating the instant at which the mandible impacts the object, the position of the contact and the exerted force. The algorithms that estimate these values are based on an accurate model of the beak, which is developed in this section.

The lower mandible is a rigid link. Then its dynamic model is simple and no more attention will be paid to it. This section focuses on the much more involved dynamics of the upper mandible. The knowledge of this dynamics is essential in order to extract useful information from the mandible bending measurements provided by the strain gauges.

A. Hypotheses about the planar movement of the beak

Fig. 1 sketches the bending of the upper mandible in a plane perpendicular to the surface of the object at the contact point (this plane includes the origin O and the contact point p_c). In this figure, $X-Y$ is the $2D$ rotating frame of the bending plane, where X is the direction of the mandible if it were rigid; $p(x,y)$ is a generic point of the mandible in which x is the position of this point along the mandible if it were rigid and y is the deflection of the point; (x_c,y_c) are the coordinates of the contact point p_c, which is assumed invariant because the contacted object is rigid; X_0-Y_0 is the $2D$ absolute frame whose axis Y_0 defines the direction opposite to the gravity g; θ_u and θ_l are respectively the angles of the upper and lower mandibles in the absolute frame (given with respect to axis X_0); and θ_m is the opening angle of the beak, which is the difference between θ_u and θ_l. The opening angle θ_m is provided by a servo controlled motor and is known because it is measured by the encoder integrated on it. Most of these variables vary with time, which is represented by t.

Fig. 1 also mentions the mechanical characteristics of the upper mandible: E is the Young's modulus, I is the inertial moment of the beam cross section, L is the length of the beam,

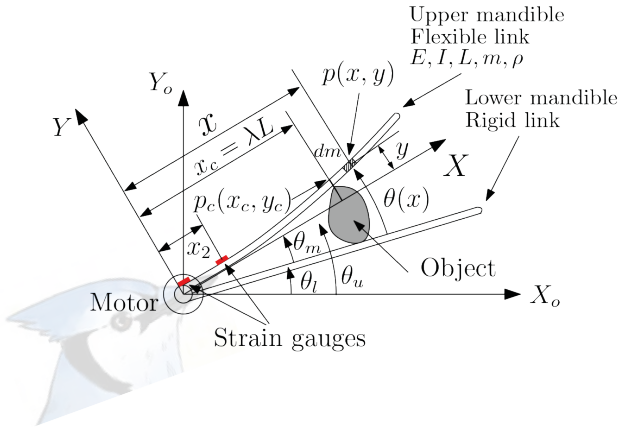

Fig. 1 Sketch of the robotic beak.

ρ is the linear density of the beam, m is the mass of the beam ($m=\rho\cdot L$) and dm is the mass of the differential element of mass. The nondimensional contact position is $\lambda = x_c/L$. The first strain gauge is placed on the base of the beam and the second one x_2 m away from the base.

The following assumptions are made about the beam that constitutes the upper mandible:

1) The maximum deflection of the beam is limited to 10% of the total beam length in order to obtain linear deflections. Then deflections y are small when compared to their corresponding x values. The deflected abscissa, therefore, has approximately the same value as the undeflected one; $arctan\left(\frac{y}{x}\right)\approx\frac{y}{x}$; and x and y become the coordinates of a point of the deflected beam expressed in the frame $X-Y$. This assumption is justified because: a) the value of 10%, needed to assume a geometrically linear deflection, is commonly used in studies of beam deflections and vibrations (a justification can be found in [26]), b) though free movements can perform fast trajectories, deflections are lower than this limit because the mandibles are very lightweight and, then, inertial forces are low and c) in the contact mode, the force exerted by the mandibles on the object must be high enough to allow a reliable estimation of the contact point but low enough to prevent exceeding this deflection limit.
2) The upper mandible has an uniform cross section.
3) Since the upper mandible is slender, rotatory inertia, shear deformation and internal friction are ignored.
4) The contacted object does not move during sensing.
5) The vibration associated to the first mode is much more relevant than the vibrations associated to other modes in the free movement of the upper mandible [27] and the gravitational force cannot be neglected neither in the free mandible movements or in the contact condition.

And the following assumptions are made for the contact:

1) The contacted object is rigid.
2) The contact is produced at a single point (it is often assumed in previous works about robots contacting the environment).
3) A first-order beam analysis (e.g, [28]) will be carried out on the upper mandible, i.e., the points of the mandible

are displaced by the applied forces perpendicularly to the mandible assumed being rigid.

4) Sliding of the contacting bodies relative to one another is negligible once a specific value of the grasping force has been attained, i.e. if the grasping force of the mandible on the object surpasses a specific value.
5) Since there is no deformation of the upper mandible in the X axis, longitudinal contact forces do not influence the dynamics modeled.

As consequence of the previous assumptions, the system shown in Fig. 1 has linear dynamics and the superposition principle can, therefore, be applied. Then the deflection of the upper mandible can be expressed as the addition of its transient response $y_t(x,t)$ and its steady state component $y_s(x)$ (permanent deflection of the beam assuming that the transient has vanished). They will be subsequently characterized.

B. Transient dynamics of the upper mandible in contact

If the third assumption about the beam holds, the transient can be obtained from the partial differential equation of Euler-Bernouilli beams

$$E \cdot I \cdot y_t^{''''}(x,t) + \rho \cdot \ddot{y}_t(x,t) = 0 \tag{1}$$

where ($'$) represents the spatial derivative with respect to x and ($\dot{}$) the time differentiation.

Transient $y_t(x,t)$ is obtained from (1) by assuming that the base end of the upper mandible is clamped to the motor and the point at which the mandible comes into contact with the object is aligned with X axis. Then the differential equation (1) is solved using the following contour conditions [16]:

$$\begin{aligned} &y_t(0,t) = 0, \quad y_t^{'}(0,t) = 0, \quad y_t^{''}(L,t) = 0, \\ &y_t^{'''}(L,t) = R_m \cdot \ddot{y}_L(L,t), \quad y_t(x_c,t) = 0, \\ &y_t^{'}(x_c^+,t) = y_t^{'}(x_c^-,t), \quad y_t^{''}(x_c^+,t) = y_t^{''}(x_c^-,t) \end{aligned} \tag{2}$$

where x_c^- means that x approaches x_c from the left, x_c^+ means that x approaches x_c from the right, and $R_m = m_t/m$ is the ratio between the mass of the payload m_t and the mass of the beam, m. In our case, $R_m = 0$, because the upper mandible has no payload at its free tip, i.e, $m_t = 0$. Equations (1)(2) can be solved by using the separation of variables [29] yielding a general solution of the form $y_t(x,t) = \sum_{j=1}^{\infty} A_j \cdot \varphi_j(x) \cdot \sin(\omega_j \cdot t + \alpha_j)$ where $\varphi_j(x)$ is the natural mode, ω_j is the angular frequency, A_j is the amplitude and α_j is the phase angle of the $j-th$ vibration mode.

Upon introducing the variable $\beta_j^2 = \omega_j \cdot \sqrt{\frac{\rho}{E \cdot I}}$, the frequencies of the vibration modes are the solutions of the equation

$$\begin{aligned} &\cosh(\beta_j(L-x_c))[\sin(\beta_j x_c)\cosh(\beta_j x_c) - \sin(\beta_j(L-x_c))] + \\ &\cos(\beta_j(L-x_c))[\sinh(\beta_j(L-x_c)) - \sinh(\beta_j x_c)\cos(\beta_j x_c)] + \\ &\quad \cos(\beta_j x_c)[\sin(\beta_j x_c) - \cos(\beta_j x_c)\sinh(\beta_j x_c)] = 0 \end{aligned} \tag{3}$$

The derivation of this model can be found in [16].

C. Steady state of the upper mandible in contact condition

Component $y_s(x)$ can be obtained from the Euler-Bernouilli deflection equation of a static beam given by

$$E \cdot I \cdot y_t^{''''} + \rho \cdot g \cdot \cos(\overline{\theta}_u) = 0 \tag{4}$$

where $\overline{\theta}_u$ is the steady state value of the angle of the upper mandible with respect to the horizontal axis X_0, assuming that neither external forces, nor internal forces or moments are applied, i.e, assuming that the mandible is rigid. This angle is supposed to be known since it is the sum of the angle of the lower mandible, which is known, and the angle of the motor. Its solution is a four degree polynomial in x.

The contour conditions (2) are taken into account again in order to solve the differential equation (4), with the exception that condition $y_t(x_c,t) = 0$ is substituted by $y_s(x_c^+) = y_s(x_c^-) = y_c$ and the argument t is removed from variable y. These new eight contour conditions impose a polynomial on the interval before x_c and another on the interval after it, as $y_{s,i}(x) = -\frac{K}{24} \cdot x^4 + \frac{a_i}{6} \cdot x^3 + \frac{b_i}{2} \cdot x^2 + c_i \cdot x + d_i, \quad x \in \mathbf{I}_i$, where $i = 1,2$, $\mathbf{I}_1 = [0, x_c]$, $\mathbf{I}_2 = [x_c, L]$ and $K = \frac{g \cdot \rho \cdot \cos(\overline{\theta}_u)}{E \cdot I}$. The eight parameters of these two polynomials are obtained from the eight contour conditions after some calculations:

$$\begin{aligned} a_1 &= \tfrac{3}{2} \cdot \tfrac{K \cdot L}{x_c} \cdot \left(x_c - \tfrac{L}{2}\right) - 3 \cdot \tfrac{y_c}{x_c^3} - \tfrac{K}{8} \cdot x_c \\ b_1 &= K \cdot L \cdot \left(x_c - \tfrac{L}{2}\right) - a_1 \cdot x_c; \quad c_1 = 0; \quad d_1 = 0 \\ a_2 &= K \cdot L; \quad b_2 = -\tfrac{K}{2} \cdot L^2; \quad c_2 = -\tfrac{3 \cdot d_2}{x_c} \\ d_2 &= -\tfrac{y_c}{2} - \tfrac{1}{8} \cdot K \cdot L^2 \cdot x_c^2 + \tfrac{1}{12} \cdot K \cdot L \cdot x_c^3 - \tfrac{K}{48} \cdot x_c^4 \end{aligned} \tag{5}$$

D. Steady state forces and moments

The steady state moments Γ_s and forces F_s at a point x of the upper mandible in the two intervals of the beam are:

$$\begin{aligned} \Gamma_{s,i}(x) &= E \cdot I \cdot y^{''}(x) = E \cdot I \cdot \left(-\tfrac{K}{2} \cdot x^2 + a_i \cdot x + b_i\right) \\ F_{s,i}(x) &= -E \cdot I \cdot y^{'''}(x) = -E \cdot I \cdot (-K \cdot x + a_i), \quad i = 1,2 \end{aligned} \tag{6}$$

The reaction force F_c exerted by the object on the beam yields

$$F_c = F_{s,1}(x_c) - F_{s,2}(x_c) = E \cdot I \cdot (a_2 - a_1) \tag{7}$$

Remark: According to expressions (6), $\Gamma_{s,2}(x)$ and $F_{s,2}(x)$ do not depend on the contact point p_c since a_2 and b_2 do not depend on x_c nor y_c. Then installing moment or force sensors in $\mathbf{I}_2$ is useless in order to estimate the contact point x_c or the exerted force F_c. The sensors have to be therefore installed in the interval $\mathbf{I}_1$ and, since x_c is a priori unknown, they have to be placed close to the base of the beam.

Moment $\Gamma_{s,1}(x)$ can be expressed as a function of F_c as follows. Substituting the value of a_2 given by (5) in equation (7) and equating a_1 yields $a_1 = K \cdot L - \frac{F_c}{E \cdot I}$, which substituted in the expression of b_1 given by (5) yields $b_1 = \frac{F_c \cdot x_c}{E \cdot I} - \frac{K \cdot L^2}{2}$. Substituting these two expressions and the value of K in the upper equation of (6) with $i = 1$, and operating gives

$$\Gamma_{s,1}(x) = F_c \cdot (x_c - x) - \frac{K \cdot E \cdot I}{2} \cdot (L - x)^2 \tag{8}$$

IV. Estimation Algorithm

The method with which to estimate the instant at which the beak's upper mandible impacts the object, the position of the contact and the exerted force is developed here.

A. Detection of the impact instant t_c

For simplicity, in this paper the estimator proposed in [20] and [25] is used, which attains very good results. This

algorithm is based on detecting when the residue of the torque at the base of the beak, i.e., the difference between the torque measured at the base by the strain gauges $\Gamma_1(0,t)$ and its value predicted by the model $\Gamma_1^p(0,t)$, exceeds a threshold. This mechanism is very simple since $\Gamma_1^p(0,t)$ can be easily calculated using the dynamic model of the link in free motion, see [25]. If this difference were noticeable, it would mean that an external force is being exerted at the tip, and a contact has happened. Thus, the detection condition yields $|\Gamma_1^p(0,t)-\Gamma_1(0,t)|>\gamma$, where γ is a threshold experimentally determined, which is independent of the contact point. The threshold is given by the maximum residual obtained during free movements plus a security margin of 50%.

B. Estimator based on the steady state deflections

This section presents the new algorithm that estimates the point of the flexible beam that comes into contact with an object and the reaction force produced. It is based on the information collected by the two strain gauges located at $x_1=0$ and x_2. With them, the moments at these points can be estimated, which would be given by expression (8) if $x_2<x_c$. Let us represent by Γ_1 and Γ_2 the measurements provided by the strain gauges at points x_1 and x_2 respectively. They can be expressed as:

$$\begin{aligned}\Gamma_1 &= \Gamma_{s,1}(x_1=0)+\xi_1=\Gamma_c-\tfrac{K\cdot E\cdot I}{2}\cdot L^2+\xi_1\\ \Gamma_2 &= \Gamma_{s,1}(x_2)+\xi_2=\Gamma_c-F_c\cdot x_2-\tfrac{K\cdot E\cdot I}{2}\cdot(L-x_2)^2+\xi_2\end{aligned} \tag{9}$$

where $\Gamma_c=F_c\cdot x_c$ is the torque produced at the base of the beam by the reaction force of the object, and ξ_1 and ξ_2 are disturbances in the measurements of the strain gauges at x_1 and x_2 respectively, as e.g., offsets and high frequency noises. The upper equation of (9) yields an estimator of Γ_c:

$$\Gamma_{c,e}=\Gamma_1+\frac{K\cdot E\cdot I}{2}\cdot L^2=\Gamma_c+\xi_1 \tag{10}$$

and substracting the two equations (9) and solving for F_c yields its estimator, namely $F_{c,e}$, as

$$F_{c,e}=\frac{\Gamma_1-\Gamma_2+K\cdot E\cdot I\cdot x_2\cdot(L-0.5\cdot x_2)}{x_2}=F_c+\frac{\xi_1-\xi_2}{x_2} \tag{11}$$

Then an estimation of the contact point x_c is obtained dividing equations (10) and (11) and reads

$$x_{c,e}=\Gamma_{c,e}/F_{c,e} \tag{12}$$

Recall that K depends on the angle of the upper mandible in the steady-state $\overline{\theta}_u$. Angle θ_u is given by $\theta_u=\theta_l+\theta_m$. In this expression, the angle of the lower mandible with respect to the direction of the gravity, θ_l, is obtained from the pitch angle of the ornithopter measured by the *IMU* installed on our flapping wing robot [2] and the relative angle between the lower mandible of the beak and the body of the ornithopter (this angle is exactly known after its manufacturing). Moreover, θ_m is given by the encoder embedded in the motor of the beak. Noisy measurements are not a problem because signals are passed through low-pass filters. Then, the estimation of the exerted force, $F_{c,e}$ and the contact point $x_{c,e}$ can be obtained from (11) and (12) using the properties of the flexible beam, the position of the second strain gauge, x_2, the torque measurements Γ_1, Γ_2 and the steady-state angle of the upper mandible $\overline{\theta}_u$.

Expression (11) shows that if the second strain gauge is installed close to the first one, i.e., $x_2\to 0$, the effect of the measurement disturbances on the estimation of F_c grows rapidly due to the term $\frac{\xi_1-\xi_2}{x_2}$. Then, the effect of ξ_1 and ξ_2 on the estimation of F_c and, consequently, on the estimation of x_c–according to (12), $x_{c,e}$ depends on $F_{c,e}$- is reduced if the second strain gauge is placed as far as possible from the origin, i.e., x_2 is as high as possible. Moreover, since it is assumed that $x_c>x_2$, x_2 cannot be too high in order to do not reduce excessively the grasping zone. As consequence of the previous considerations, once the grasping zone $[\hat{x}_c,L]$ has been defined, the second strain gauge must be installed as close as possible to the lower limit $\hat{x}_c$ of that interval.

The stages of the estimation method are: 1) the servo moves freely the flexible beam in a controlled manner until it hits an object; 2) the algorithm of Section IV-A estimates the instant t_c at which the flexible beam impacts the object; 3) after the impact, the motor keeps pushing slightly the flexible beam against the object to increase the contact force and prevent the sliding; and 4) the estimator of the contact point and the exerted force is triggered at time $t_1=t_c+\Delta t_1$ in which Δt_1 is the estimation time plus a safety margin. The estimator is based on the expressions (11) and (12). The torque signals used in the estimator are passed through a low-pass filter that attenuates the transient dynamics and keeps only the steady-state components.

V. Simulation and Experimental validation

Experimental prototype. The experimental prototype (see Fig. 3) consists of a lightweight flexible link ($m=5.5$ g and $l=300$ mm) which is attached at one of its ends to a micro motor (12 g weight) based on the Pololu micro metal motors gears with high reduction ratio (n=250).

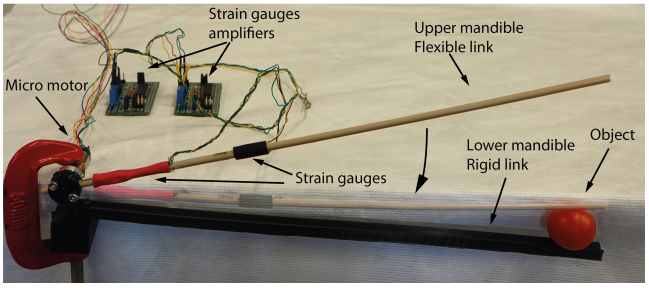

Fig. 3 Photograph of the prototype.

The flexible link is a circular cross section bar with a diameter of 4.3 mm made of Polyetheretherketone (PEEK) which is a thermoplastic polymer which has excellent mechanical properties ($E=3.33\times10^9$ Nm) maintained to high temperatures. Also, this material is easily deformable and its density is considerably low. The motor rotates the system with elevation movements and has embedded an incremental optical encoder that measures its angular position. The system also has two strain gauges (KFGS 3-120-C1-27, KYOWA) located at

TABLE I Simulated results: without considering gravity $(x^*_{c,e}, F^*_{c,e})$ and considering gravity $(x_{c,e}, F_{c,e})$.

$x_c(mm)$	90	120	150	180	210	240	270	290
$x^*_{c,e}(mm)$	85.8	114.8	145.8	179.4	219.9	268.8	333	373.2
$x_{c,e}(mm)$	88.2	118.4	148.5	178.8	209	239.1	269.4	287.2
$F_c(N)$	1.15	0.726	0.43	0.28	0.197	0.148	0.114	0.1
$F^*_{c,e}(N)$	1.05	0.657	0.376	0.23	0.15	0.101	0.068	0.056
$F_{c,e}(N)$	1.13	0.703	0.42	0.275	0.195	0.147	0.113	0.1

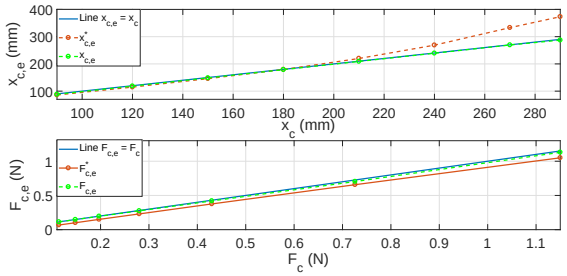

Fig. 2 Simulated results

the base, $x_1 = 0$, and at the point $x_2 = 78.75$ mm, following the results obtained in Section IV-B. They are connected to gauge amplifiers, INA 125P (8 g weight) which have been thoroughly calibrated to allow us to measure the torque at these points. This x_2 value is a good compromise between minimizing the effect of measurement disturbances and achieving an important grasping zone $[78.75, 300]$ mm. The data acquisition sampling time is 5 ms.

Simulated results. Simulations using the finite elements software package Adams together with Matlab/Simulink have been carried out to verify the effectiveness of the proposed algorithm and assess some aspects of the method. The properties of the flexible beam were used in the simulations, in which our beam was modeled by 120 flexible elements. The beam estimators proposed in expressions (11) and (12) are tested in attitude movements where the gravity effect is important. To estimate these values, both variables are passed through a first order low-pass filter in order to attenuate the vibration and get the steady-state values.

Considering the operating range $\lambda \in [0.3, 1]$, the natural frequencies during the contact mode were obtained from equation (3) using the properties of our flexible beam. Then, the range of the first vibration frequency of the beak in function of the normalized contact point λ is [116.2, 427.3] rad/s. A cutoff frequency of $\omega_c = 15$ rad/s was chosen which is about seven times lower than the inferior limit of this frequency range. This value allows a reasonable filtering of the vibration for all the contact points.

In those simulations, the system is moved until it hits the object. Once the impact is detected, the motor continues pushing the object with a determined force. In the simulations, the contact was made at positions from 90 mm to 300 mm with increments of 30 mm. The results of the estimations are shown in Table I. It presents the differences between using the estimator without considering the gravity effect, $K = 0$, $(x^*_{c,e}, F^*_{c,e})$ and using our estimator which considers the gravity effect $(x_{c,e}, F_{c,e})$. The results show the importance of using a model with distributed mass where the gravity effect is considered. Fig. 4 shows the results of a simulation where the flexible beam hits the object and then continues pushing the object with different motor position values in order to verify that the proposed algorithm is robust to the position of the motor in $x_c = 240$ mm. These simulations demonstrate the importance of considering the gravity in the estimator. Contact points close to the base are well estimated by both estimators but, from $x_c = 180$ mm to the end of the beam (see Table I), the gravity has to be considered in order to attain good accuracy in the estimation of the contact point and the exerted force. Our estimator is robust to the motor position and the results show the high accuracy of the contact point and the exerted force estimations: a maximum error in the contact point of 2 mm (around 0.7% the length of the beam) and an error in the exerted force of 0.02 N (2% the real value). Table I and Fig. 2 show that the estimation of the exerted force considering the gravity is much better, note that it almost overlaps the ideal case in blue and without gravity has a bias. The estimated values of the force are bigger when considering the gravity than without it, the latter corresponding to $K = 0$ in equation (11) so it does not add value to the estimation.

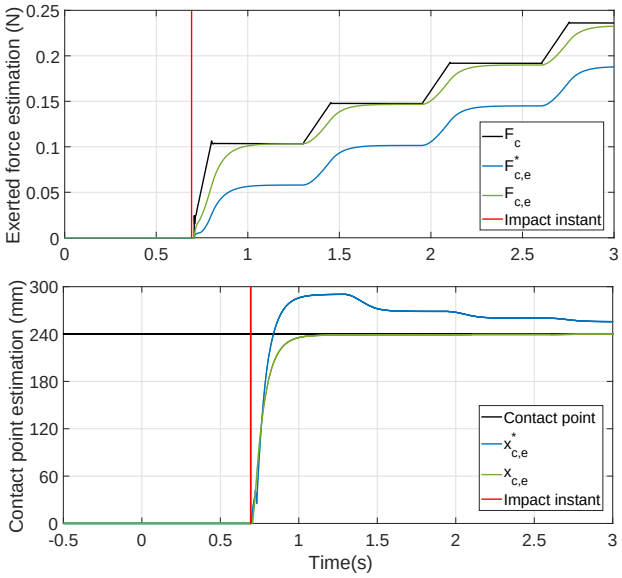

Fig. 4 Contact distance and exerted force estimations.

Experimental results. Experiments have been carried out with this prototype that demonstrate the efficiency and robustness of the proposed technique for different rigid objects. The real value of the contact point is known placing the object in determined positions whereas the real exerted force in the contact point is calculated by using a electronic weighing machine with a precision of 0.01 N. The object is located above the scale and once the flexible beam hits the object, the scale measures the equivalent force in the contact point. An efficient control system for motors that move flexible links has been implemented in the experiments (see [19], [27]). This controller does not change during the complete maneuver, i.e., its parameters remain invariant during the free and contact

motions. The position of the motor θ_m is measured by an encoder and the torques Γ_1 and Γ_2 by the strain gauges with the amplifiers. The upper mandible is moved on a vertical plane until it hits an object. Then the impact instant is detected by the algorithm of Subsection IV-A, where a threshold of 0.01 Nm has been used and experimentally estimated. Once, the system detects the impact, the algorithm of Subsection IV-B is launched to estimate the contact point and the exerted force, and the mandible pushes on the object by moving the motor forward an angle of 10° (angle increment with respect to the contact angle). This angle increment produces a deflection on the beak that yields a grasping force that is high enough to avoid the sliding and low enough not to surpass the deflection of 10% in any case. Given an increment of the motor angle after the impact, the force exerted by the beak on an object diminishes as the contact point moves away from the motor. That motor angle increment has been therefore obtained experimentally taking into account these considerations in the force exerted at the tip of the beak. Again, a low-pass filter with $\omega_c = 15$ rad/s cutoff frequency was used experiments. In the experiments, the contact was made at positions from 120 mm to 300 mm with increments of 20 mm. Fig. 5 shows the torques provided by the strain gauges. It also shows noise level and the vibration during the contact (both attenuated by the filter) and the detection of the impact instant.

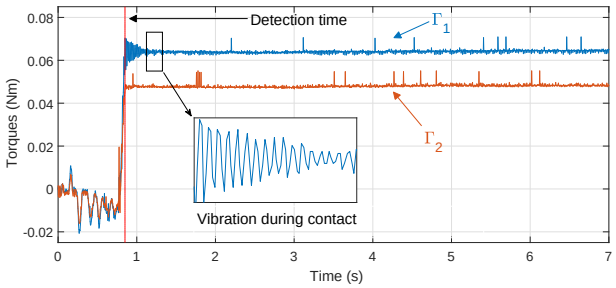

Fig. 5 Measured torques in the two points of the link.

Fig. 6 shows the estimates given by expressions (11) and (12) of the contact point, $x_{c,e}$, and the exerted force, $F_{c,e}$. Results of experiments with the object located in four different positions are reported. These show the fast convergence of the estimations and that the vibrations have been properly removed by the low-pass filter. The real values of the contact point, the steady state measurement of the force (orange line) and their estimations (blue line) are also drawn. Admissible zones of convergence have been highlighted for the contact point estimation ($x_c \pm 10$ mm) and for the exerted force estimation ($F_c \pm 0.03$ N). These results demonstrate the robustness of our algorithm to changes in the contact point and the force exerted on the object. Our estimation algorithm is fast, it only has a time delay between 0.3 s and 0.45 s (the difference between the time at which the impact is detected and the time at which the estimation of the contact point enters the admissible zone of convergence).

Finally, Table II and Fig. 7 show the estimation of the contact points, $x_{c,e}$, and the exerted forces, $F_{c,e}$, provided by

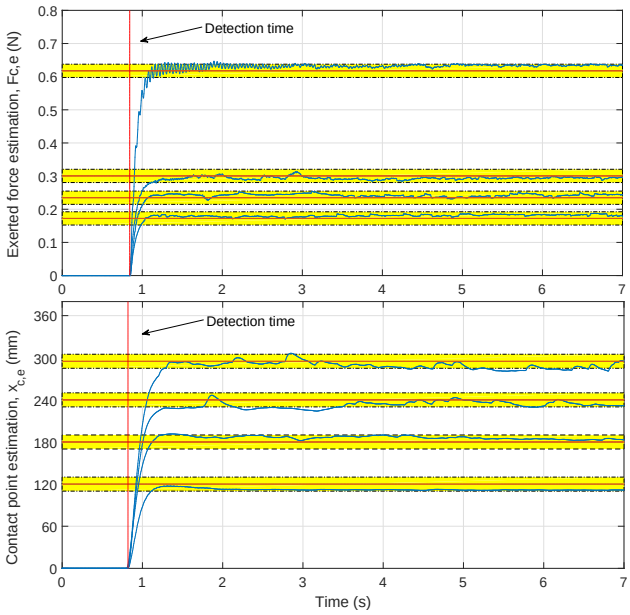

Fig. 6 Contact point distance and exerted force estimation.

our algorithm versus their real values x_c and F_c. Estimates of the contact point show a maximum error of 8 mm and a mean error of 5 mm, which are respectively the 2.7% and 1.7% of the length of the flexible link. Estimates of the force show a maximum error of 0.03 N (5% of its real value). These results also show that the accuracy of our estimator is similar to the former works presented in Section II, but meeting the aerial robotics requirements explained in the Introduction.

VI. Conclusions

This paper proposes a very lightweight sensor system that emulates a birds beak to allow flapping aerial robots to perform manipulation and grasping tasks. The robotic beak is composed of an upper and a lower mandible. The upper one constitutes the sensing system and is a flexible beam actuated at the base by a micro motor. The estimation is performed sequentially, first detecting the impact of the beak on the object and, subsequently, estimating the contact point and the exerted force. Our sensing system outperforms previous designs because the algorithm is fast with a very low computational load and the weight/size is very light/small. This sensor system meets all the demanding requirements imposed by aerial robots with flapping-wings. The effectiveness of the proposed method has been validated through finite element simulations and an experimental prototype. The simulations demonstrate the high precision of the methodology and validate the assumptions made in the dynamic model. On the other hand, the experimental results show the effectiveness of the algorithm in real applications obtaining a maximum error in the contact point of 2.7% the length of the flexible beam and a 5% in the exerted force. Thus, the precision is similar to the available schemes relying on force/torque sensors.

Future research will address the development of a force control strategy for grasping tasks.

TABLE II Contact detection results with the prototype.

$x_c(mm)$	120	140	160	180	200	220	240	260	280	295
$x_{c,e}(mm)$	112	132	153	187	208	215	237	262	288	293
Error $x_{c,e}(mm)$	8	8	7	7	8	5	7	2	8	2
$F_c(N)$	0.59	0.52	0.4	0.3	0.29	0.26	0.24	0.23	0.19	0.18
$F_{c,e}(N)$	0.62	0.49	0.38	0.29	0.28	0.28	0.25	0.24	0.17	0.19
Error $F_{c,e}(N)$	0.03	0.03	0.02	0.01	0.01	0.02	0.01	0.01	0.02	0.01

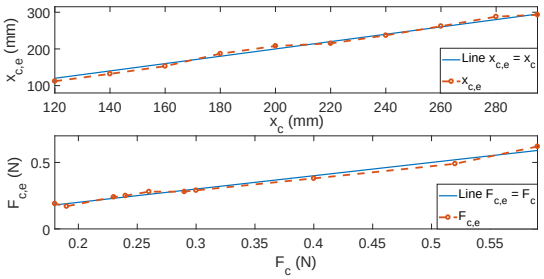

Fig. 7 Contact point and exerted force estimation

REFERENCES

[1] H2020-EU ERC Advanced Grant 788247, "General compliant aerial robotic manipulation system integrating fixed and flapping wings to increase range and safety, 2018."

[2] R. Zufferey, J. Tormo-Barbero, M. M. Guzmán, F. J. Maldonado, E. Sanchez-Laulhe, P. Grau, M. Pérez, J. Á. Acosta, and A. Ollero, "Design of the high-payload flapping wing robot e-flap," *IEEE Robotics and Automation Letters*, vol. 6, no. 2, pp. 3097–3104, 2021.

[3] D. Feliu-Talegon, J. Á. Acosta, A. Suarez, and A. Ollero, "A bio-inspired manipulator with claw prototype for winged aerial robots: Benchmark for design and control," *Applied Sciences*, vol. 10, no. 18, p. 6516, 2020.

[4] D. Feliu-Talegon, J. Á. Acosta, and A. Ollero, "Control aware of limitations of manipulators with claw for aerial robots imitating bird's skeleton," *IEEE Robotics and Automation Letters*, vol. 6, no. 4, pp. 6426–6433, 2021.

[5] M. Salman and M. J. Pearson, "Whisker-ratslam applied to 6d object identification and spatial localisation," in *Conference on Biomimetic and Biohybrid Systems*, pp. 403–414, Springer, 2018.

[6] M. Fend, "Whisker-based texture discrimination on a mobile robot," in *European Conference on Artificial Life*, pp. 302–311, Springer, 2005.

[7] M. J. Pearson, C. Fox, J. C. Sullivan, T. J. Prescott, T. Pipe, and B. Mitchinson, "Simultaneous localisation and mapping on a multi-degree of freedom biomimetic whiskered robot," in *2013 IEEE Int. Conf. Robotics and Automation*, pp. 586–592, IEEE, 2013.

[8] S. Hellbach, A. F. Krause, and V. Dürr, "Feel like an insect: a bio-inspired tactile sensor system," in *International Conference on Neural Information Processing*, pp. 676–683, Springer, 2010.

[9] P. V. Alvarado, V. Subramaniam, and M. Triantafyllou, "Performance analysis and characterization of bio-inspired whisker sensors for underwater applications," in *Proc. IEEE/RSJ Int. Conf. Intell. Robots Syst, 2013*, pp. 5956–5961, IEEE, 2013.

[10] J. Becedas, I. Payo, and V. Feliu, "Two-flexible-fingers gripper force feedback control system for its application as end effector on a 6-dof manipulator," *IEEE Trans. Robot*, vol. 27, no. 3, pp. 599–615, 2011.

[11] A. Garcia and V. Feliu, "Force control of a single-link flexible robot based on a collision detection mechanism," *IEE Proceedings-Control Theory and Applications*, vol. 147, no. 6, pp. 588–595, 2000.

[12] E. Magrini, F. Flacco, and A. De Luca, "Estimation of contact forces using a virtual force sensor," in *Proc. IEEE/RSJ Int. Conf. Intell. Robots Syst, 2014*, pp. 2126–2133, IEEE, 2014.

[13] M. Kaneko, N. Kanayama, and T. Tsuji, "Active antenna for contact sensing," *Robot and Autom, IEEE Trans.*, vol. 14, no. 2, pp. 278–291, 1998.

[14] C. F. Castillo-Berrio and V. Feliu-Batlle, "Vibration-free position control for a two degrees of freedom flexible-beam sensor," *Mechatronics*, vol. 27, pp. 1–12, 2015.

[15] N. H. Nguyen, T. D. Ngo, D. Q. Nguyen, and V. A. Ho, "Contact distance estimation by a soft active whisker sensor based on morphological computation," in *Proc. Int. Conf.on Biomedical Robot and Biomechatronics*, pp. 322–327, IEEE, 2020.

[16] N. Ueno, M. M. Svinin, and M. Kaneko, "Dynamic contact sensing by flexible beam," *Mechatronics, IEEE/ASME Transactions on*, vol. 3, no. 4, pp. 254–264, 1998.

[17] T. Clements and C. D. Rahn, "Three-dimensional contact imaging with an actuated whisker," *Robotics and Automation, IEEE Transactions on*, vol. 22, no. 4, pp. 844–848, 2006.

[18] C. F. Castillo Berrio, *Diseño, modelado y control de antenas sensoras flexibles de dos grados de libertad*. Universidad de Castilla-La Mancha, 2016.

[19] V. Feliu-Batlle, D. Feliu-Talegon, and C. F. Castillo-Berrio, "Improved object detection using a robotic sensing antenna with vibration damping control," *Sensors*, vol. 17, no. 4, pp. 852–879, 2017.

[20] L. Mérida-Calvo, D. Feliu-Talegón, and V. Feliu-Batlle, "Improving the detection of the contact point in active sensing antennae by processing combined static and dynamic information," *Sensors*, vol. 21, no. 5, p. 1808, 2021.

[21] A. De Luca and R. Mattone, "Sensorless robot collision detection and hybrid force/motion control," in *Proceedings of the 2005 IEEE Int. Conf. on robotics and automation*, pp. 999–1004, IEEE, 2005.

[22] A. De Luca, A. Albu-Schafier, S. Haddadin, and G. Hirzinger, "Collision detection and safe reaction with the dlr-iii lightweight manipulator arm," *Proc. IEEE/RSJ Int. Conf. Intell. Robots Syst, 2006*, pp. 1623–1630, 2006.

[23] J. Malzahn and T. Bertram, "Collision detection and reaction for a multi-elastic-link robot arm," *Proceedings of the 19 World Congress of the International Federation of Automatic Control (IFAC)*, 2014.

[24] D. Feliu-Talegon, R. Cortez-Vega, and V. Feliu-Batlle, "Improving the contact instant detection of sensing antennae using a super-twisting algorithm," in *2020 IEEE International Conference on Robotics and Automation (ICRA)*, pp. 7885–7890, IEEE, 2020.

[25] D. Feliu-Talegon, V. Feliu-Batlle, I. Tejado, B. M. Vinagre, and S. H. HosseinNia, "Stable force control and contact transition of a single link flexible robot using a fractional-order controller," *ISA transactions*, vol. 89, pp. 139–157, 2019.

[26] T. Beléndez, C. Neipp, and A. Beléndez, "Large and small deflections of a cantilever beam," *Eur. J of physics*, vol. 23, no. 3, p. 371, 2002.

[27] D. Feliu-Talegon, V. Feliu-Batlle, and C. F. Castillo-Berrio, "Motion control of a sensing antenna with a nonlinear input shaping technique," *RIAI-Revista Iberoamericana de Automática e Informática Industrial*, vol. 13, no. 2, pp. 162–173, 2016.

[28] B. Davison and G. Owens, *Steel designers manual*. Wiley-Blackwell, 2012.

[29] L. Meirovitch, *Analytical methods in vibrations*. Macmillan, 1967.